

A CAUSAL FRAMEWORK FOR ALIGNING IMAGE QUALITY METRICS AND DEEP NEURAL NETWORK ROBUSTNESS

Nathan Drenkow^{1,2}

¹The Johns Hopkins University Applied Physics Laboratory
Laurel, MD USA

Mathias Unberath²

²The Johns Hopkins University
Baltimore, MD USA

ABSTRACT

Image quality plays an important role in the performance of deep neural networks (DNNs) and DNNs have been widely shown to exhibit sensitivity to changes in imaging conditions. Large-scale datasets often contain images under a wide range of conditions prompting a need to quantify and understand their underlying quality distribution in order to better characterize DNN performance and robustness. Aligning the sensitivities of image quality metrics and DNNs ensures that estimates of quality can act as proxies for image/dataset difficulty independent of the task models trained/evaluated on the data. Conventional image quality assessment (IQA) seeks to measure and align quality relative to human perceptual judgments, but here we seek a quality measure that is not only sensitive to imaging conditions but also well-aligned with DNN sensitivities. We first ask whether conventional IQA metrics are also informative of DNN performance. In order to answer this question, we reframe IQA from a causal perspective and examine conditions under which quality metrics are predictive of DNN performance. We show theoretically and empirically that current IQA metrics are weak predictors of DNN performance in the context of classification. We then use our causal framework to provide an alternative formulation and a new image quality metric that is more strongly correlated with DNN performance and can act as a prior on performance without training new task models. Our approach provides a means to directly estimate the quality distribution of large-scale image datasets towards characterizing the relationship between dataset composition and DNN performance.

1 INTRODUCTION

Ensuring the robustness of deep neural networks (DNNs) to real-world imaging conditions is crucial for safety- and cost-critical applications. Extensive research has shown that DNNs remain sensitive to natural distortions (Taori et al., 2020; Djolonga et al., 2021; Ibrahim et al., 2022; Geirhos et al., 2021) despite efforts to close the gap between performance on clean and naturally-distorted images. While much effort has focused primarily on the design and optimization of robust DNNs, there is now growing interest in developing a deeper understanding of how the properties of the image data itself influence robustness during training and evaluation (Ilyas et al., 2022; Lin et al., 2022; Pavlak et al., 2023).

Since image quality is known to influence DNN behavior, a first step in analyzing image data is to examine the relationship between image quality (IQ) and DNN robustness. Here *quality* describes the absence of distortion but more generally relates to the ability to extract task-relevant information from the image. Image *quality* and *difficulty* are closely related where quality measures properties of the imaging conditions while difficulty involves content and composition in addition to the conditions. In the ideal case, image quality metrics will strongly correlate with task DNN performance generally while remaining independent of knowledge or assumptions about specific downstream task models that will consume the data. Despite decades of research into IQ metrics, we examine for the first time in depth the explicit connection between IQ metrics and task DNN performance. *In particular, the primary goal of this work is to provide a framework for identifying and analyzing the conditions under which IQ metrics and DNN performance are correlated.*

In providing a means to establish a link between IQ and DNN performance, our method enables new pathways for quantitatively analyzing dataset composition. Using IQ metrics as a proxy for DNN performance, we can estimate the quality distribution of datasets to understand how the range of “easy” to “hard” images influences observed DNN robustness. This becomes increasingly useful as image datasets continue to grow in size to the extent that the cost and feasibility of using human annotators to assess and annotate properties of each data point is becoming intractable. With pre-training datasets for foundation models and other large-scale vision models approaching hundreds of millions to billions of images (Radford et al., 2021; Sun et al., 2017; Schuhmann et al., 2022), new automated methods for analysis are needed for quantitatively assessing dataset composition.

In this work, we focus specifically on *natural robustness* which considers how images are distorted due to real-world factors such as lighting, weather, sensor settings, and/or motion. Image quality assessment (IQA) metrics have been developed over several decades of research (Wang & Bovik; Xu et al., 2017; Wang, 2004; Agnolucci et al., 2024) and provide quantitative measures of quality calibrated with respect to human perceptual judgments. To the best of our knowledge, little work has been done to understand how these IQA metrics can help relate image difficulty and DNN performance. To make this connection explicit, we state our primary research question: **What is the extent of the relationship between IQ and DNN performance metrics?**

Contributions To answer this question, our work makes the following contributions:

- Our primary contribution is a causal framework for analyzing the relationship between image quality and DNN performance in a range of IQA settings
- We use the framework to establish theoretically and empirically the independence of image quality and DNN performance under general conditions
- We identify specific conditions under which IQA metrics can be predictive of DNN performance
- We conduct a first-of-its-kind evaluation of the relation between conventional IQ metrics and DNN performance and find that conventional metrics are weakly predictive of performance
- We use the framework in the context of image classification tasks to develop a new task-guided IQA metric that enables quantitative assessments of image quality that are strongly predictive of downstream DNN task performance
- We show that our framework and novel metric provide the means to expose subtle differences in dataset quality distributions that directly impact on DNN performance

2 RELATED WORK

Image Quality Assessment Image quality assessment has been long-studied in the computer vision and image processing literature. Full Reference IQA (FR-IQA) (Wang, 2004; Zhang et al., 2011; 2018) assume the availability of a reference or “clean” image against which the test image is compared and the quality is measured. In contrast, the No Reference IQA (NR-IQA) (Mittal et al., 2012; Wang et al., 2022; Agnolucci et al., 2024) setting (aka Blind IQA) uses only features of the test image to estimate a quality score. In both settings, conventional IQA methods are calibrated and compared against human perceptual judgments of quality such as Mean Opinion Scores (MOS). These measures are task-agnostic and humans are not required to make judgments about the content of the image but only to measure subjective “quality” (typically on a scale of 1-5, Poor-High). This motivates our investigation into whether these metrics can also provide task-relevant assessments of image quality.

Relationship of DNNs and human perception A key question of this work centers on whether IQA metrics calibrated against human MOS are sensitive to any of the same image features that DNNs use for downstream tasks. Outside of the IQA literature, prior works have shown differences in humans and DNNs in the context of shape/texture bias (Geirhos et al., 2018; Hermann et al., 2019), shortcut learning (Geirhos et al., 2020; Zech et al., 2018; Brown et al., 2023; Ong Ly et al., 2024), and error consistency (Geirhos et al., 2021; Wichmann & Geirhos, 2023), but the question remains open whether IQA metrics aligned with human MOS correlate with DNN performance.

Dataset difficulty/pruning Our work is strongly motivated by the growing interest in automated methods for dataset analysis. In particular, new methods focus on dataset pruning (Tan et al., 2023; He et al., 2023; Abbas et al., 2024), identifying difficult/important examples (Kwok et al., 2024;

Ilyas et al., 2022) or data slices (Eyuboglu et al., 2022; Chung et al., 2019; Sohoni et al., 2020; Chen et al., 2019), and dataset auditing for shortcuts (Pavlak et al., 2023). Other results have shown that understanding dataset composition matters for analyzing model robustness (Ibrahim et al., 2022; Drenkow & Unberath, 2023). Our work takes a positive step towards automated methods for analyzing the quality distribution of image datasets and establishing priors on DNN performance.

3 CAUSAL FRAMEWORK FOR IQA

We first provide a causal inference perspective on the IQA problem. We use causal directed acyclic graphs (DAGs) to illustrate our assumptions about the imaging generating process, quality metric, and performance metric as well as the interactions between all associated variables. This causal framework provides a means for identifying the specific conditions under which quality metrics are predictive of DNN performance.

Preliminaries We specify a causal DAG \mathcal{G} via a set of nodes \mathcal{V} and directed edges \mathcal{E} . To obtain the causal interpretation, directed edges imply a causal relationship such that for a variable/node $V \in \mathcal{V}$, V is a function of its parents ($V = f_V(pa(V), U)$ where U is an exogenous noise term).

For defining causal models in the IQA context, we start from a set of factors $A \in \mathcal{A}$ that capture the key variables in the data generating process affecting the image conditions (e.g., lighting, focal length, aperture, exposure, weather). Let $X \in \mathcal{X}$ be the resulting images, and for a task T , let $Y \in \mathcal{Y}$ be the label associated with X for the task. For this work, we focus on classification tasks where \mathcal{Y} consists of a discrete set of K classes ($\mathcal{Y} = \{1, \dots, K\}$). Our quality metric $Q : \mathcal{X} \rightarrow \mathbb{R}$ maps images to real number scores (typically in $[0, 1]$ where 1 is the highest quality). We also assume a downstream task DNN $f_\theta : \mathcal{X} \rightarrow \mathcal{Y}$ that maps images to class probabilities and is parameterized by θ . We write the predicted probabilities $\hat{Y} = f_\theta(X)$ where $\hat{Y} \in \mathbb{R}^K$. Given one-hot encoded labels Y and predictions \hat{Y} , we can compute a performance metric (e.g., accuracy) $M : \mathcal{Y} \times \mathcal{Y} \rightarrow \mathbb{R}$. In the general case and without loss of generality, we assume that \hat{Y} is the prediction from a deterministic DNN. Similarly, we also assume that Q, M are both deterministic functions of their parents in the causal DAG.

3.1 IQ METRIC DESIDERATA

Our primary motivation is to identify image quality metrics that allow us to assess the distribution of image quality in large-scale datasets and establish quality-driven priors for DNN performance independent of any specific trained task models. We propose the following desiderata for IQ metrics towards achieving these objectives.

- **D1 - Sensitive:** IQ metrics should be sufficiently sensitive to changes in image conditions
- **D2 - Blind:** IQ metrics should work in No Reference IQA (NR-IQA) settings where images are assessed *without* knowledge of a reference image captured under “clean” settings
- **D3 - Predictive:** IQ metrics should be correlated with DNN task performance
- **D4 - Task Model Agnostic:** IQ metrics should be designed/trained/calibrated without *a priori* knowledge of the downstream DNN models/architectures to be trained or evaluated on the data under consideration

The first criterion (**D1**) is a baseline condition requiring that the metric is actually sensitive to the natural conditions likely in the imaging domain. **D2** operates under the assumption that real-world datasets will not consist of pairs of clean/distorted images and will instead contain images collected in diverse conditions. **D3** stems from the idea that Q should measure general properties of the data that influence M (e.g., if Q decreases, then M should also decrease, although not necessarily at the same rate). Lastly, **D4** comes from the desire to use Q to assess the composition of the dataset *independent* of any task-specific model training and without making assumptions about the type of DNN to be trained downstream. In other words, we want to avoid IQ metrics that are biased towards specific task models and/or require pre-training on each dataset to be analyzed.

3.2 BASELINE IQA FORMULATION

We start with the baseline formulation of the IQA problem as shown in Figure 1. We assume the labels Y are determined from interpreting X and that an oracle labeling function exists such that Y can always be determined from X .

This model is a general formulation and makes no assumptions about the nature of the functions that compute Q, \hat{Y} . This causal model is also consistent with conventional NR-IQA settings (Mittal et al., 2012; Ma et al., 2018) where the determination of Q given X is based on a function calibrated to human perceptual judgment and without knowledge of the task or labels.

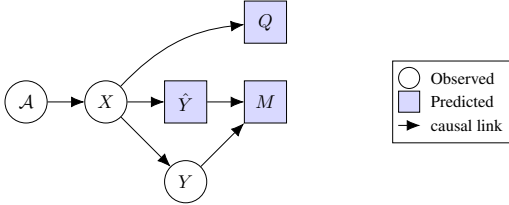


Figure 1: Causal diagram relating model accuracy (M) with IQ metrics (Q).

Conditional independence of Q, M : The causal graph of Figure 1 illustrates that under the baseline formulation, $Q \perp M | X$ and X is said to d -separate Q, M . The interpretation here is that given any image X , there is no expected relationship between Q and M by construction. This is not to say that a relationship cannot exist, but simply that there is nothing in this model that ensures it directly.

In addition to observing the d -separation of Q, M by X , we can also compute the average causal effect (ACE) of $Q \rightarrow M$. We use the potential outcomes notation $M(Q = q)$ (or $M(q)$) to indicate the value of M if Q had been set to the value of q .

$$\begin{aligned}
 ACE(Q \rightarrow M) &= \mathbb{E}[M(Q = q) - M(Q = q')] = \mathbb{E}[M(q)] - \mathbb{E}[M(q')] && \text{linearity of expectation} \\
 &= \mathbb{E}_X [\mathbb{E}[M(q)|X] - \mathbb{E}[M(q')|X]] && \text{law of total expectation} \\
 &= \mathbb{E}_X [\mathbb{E}[M(q)|Q = q, X] - \mathbb{E}[M(q')|Q = q', X]] && \text{unconfoundedness} \\
 &= \mathbb{E}_X [\mathbb{E}[M|Q = q, X] - \mathbb{E}[M|Q = q', X]] && \text{consistency} \\
 &= \mathbb{E}_X [\mathbb{E}[M|X] - \mathbb{E}[M|X]] = 0. && \text{conditional independence}
 \end{aligned}$$

The absence of causal effect and association between Q, M in this formulation suggests that, without further assumptions, traditional IQA metrics should not be predictive of DNN performance. Furthermore, while No Reference and Full Reference (FR) IQA differ in their assumptions and setup, we provide their causal models as special cases of Figure 1 in Appendix A to show that $Q \perp M | X$ holds in both cases.

3.3 SHARED FEATURES IQA FORMULATION

Ideally, we would like Q and M to become dependent when conditioning on X (i.e., we can learn about M by observing only Q). This occurs in the case where there exists a common set of features Z that are utilized both for the prediction function of \hat{Y} and the quality score Q as shown in Figure 2. This scenario does not presume a singular set of Z that serves the task model and quality metric, but rather, the Z shown here represents the intersection of features used by both. The existence of Z ensures Q, M are no longer independent given X . The primary question is whether such a Z exists or whether Q, M are related only as shown in Figure 1. An expanded discussion relating the baseline and shared features models can be found in Appendix B.

Remark: Correlation vs. Causation While we typically use causal models to estimate cause-effect relationships, a key clarification here is that we seek a weaker criterion, namely to establish the conditions under which quality and performance are *at least* correlated. Since we know that X is a common cause for both Q, M , we first want to ensure that when we estimate Q, M from X we know the conditions under which Q, M will be related via the same features of X (e.g., via Z).

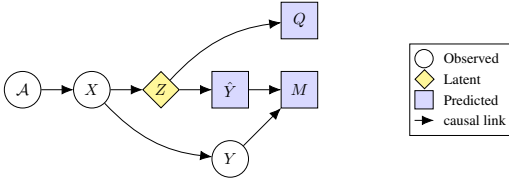


Figure 2: Causal diagram relating model accuracy (M) with IQ metrics (Q). In this case, Q and M are related via a common cause Z that represents features in the image X that influence both the prediction and quality.

4 WHAT IS THE RELATIONSHIP BETWEEN NR-IQA AND DNN PERFORMANCE METRICS?

Given the causal interpretation of IQA in §3, we now examine how conventional NR-IQA metrics relate to DNN performance. Our primary hypothesis is that if Q, M are sensitive to a common set of visual features Z derived from X (Fig. 2), then we should observe that Q is correlated with M and even predictive of M given X . Plainly stated, if image quality is high in general, then DNN performance should be similarly high (and vice versa).

We focus the following experiments on image classification tasks since they have available benchmark datasets and have been well-studied within the deep learning field. We show how our framework can be used to identify the relationship between IQA metrics and DNN performance as well as how it can guide the development of new metrics that satisfy all desiderata. For image classification, our experiments show that common NR-IQA methods are very weakly predictive of DNN performance, and while they satisfy **D1, D2, D4** of our IQ desiderata, they fail to satisfy **D3** and may not be suitable for estimating priors on DNN performance.

4.1 EXPERIMENT SETUP

In the experiments in this and subsequent sections, we use the following basic setup. In order to have precise control and knowledge of the type and severity of image distortion, we use the ImageNet validation (IN-val) and ImageNet-C (IN-C) (Hendrycks & Dietterich, 2019) datasets for evaluating IQ/performance on clean and corrupted images respectively. For reference, we provide a common corruptions causal DAG in Appendix C for comparison with the one in Figures 1 and 2.

For each experiment, we compute the IQ score (Q) and DNN correctness (M) for each image of the IN-C evaluation dataset. We use the following common and high-performing NR-IQA metrics (Q): CLIP-IQA (Wang et al., 2022), ARNIQA (Agnolucci et al., 2024), BRISQUE (Mittal et al., 2012), and Total Variation (TV). Here, CLIP-IQA and ARNIQA represent the state-of-the-art in learning-based IQA metrics while BRISQUE and TV represent conventional non-deep learning baselines. For DNNs, we evaluate the correctness (M) using pretrained ResNet34 (He et al., 2016), ConvNext-B (Liu et al., 2022), Swin-B (Liu et al., 2021) models provided via the `torchvision` package (Marcel & Rodriguez, 2010). Across all experiments, 95% confidence intervals (CI) are obtained via bootstrapping with 1000 resamples.

4.2 CORRELATION AND PREDICTABILITY OF Q, M (**D3**)

We start by examining the correlation between Q, M for NR-IQA metrics. Figure 3 shows the general relationship between Q, M where each point in the figure is the average accuracy (over 50k images) for each corruption and severity in IN-C. Similarly, Table 1 computes the Kendall Rank Correlation Coefficient (KRCC), Spearman Rank Correlation Coefficient (SRCC), and Pearson Linear Correlation Coefficient (PLCC) between IQ and average accuracy across all corruption/severity pairs (75 total).

These results provide a look at group-wise association between Q, M and the groups capture general trends in performance/IQ based on corruption type and severity. The low correlation between Q, M suggests that these NR-IQA metrics likely fall under the model described by Figure 1 where Q, M are conditionally independent given X .

We also examine the point-wise relationship between Q, M . We aggregate DNN predictions and IQ values for all images in IN-C across all corruptions/severities and then randomly split the dataset (by image ID) into 80% training and 20% testing. We train a logistic regression classifier to predict $P(M|Q)$ and test on the hold-out set. We measure the predictability of M using Area Under the Curve (AUC) and average cross-entropy (CE).

Table 1 shows that at the per-image level, Q is still weakly predictive of M (i.e., $AUC \approx 0.5$). This result is consistent with the theoretical analysis in §3 and the weak correlation observed empirically between Q, M measured at the group level. While the causal DAG in Figure 1 would suggest that conditioning on Y should not change the result, we test this empirically as follows.

We re-run the logistic regression for each label value in \mathcal{Y} separately (1000 total) and compute the mean AUC ($mAUC$) and CE (mCE) across all labels. While we observe some variability in results

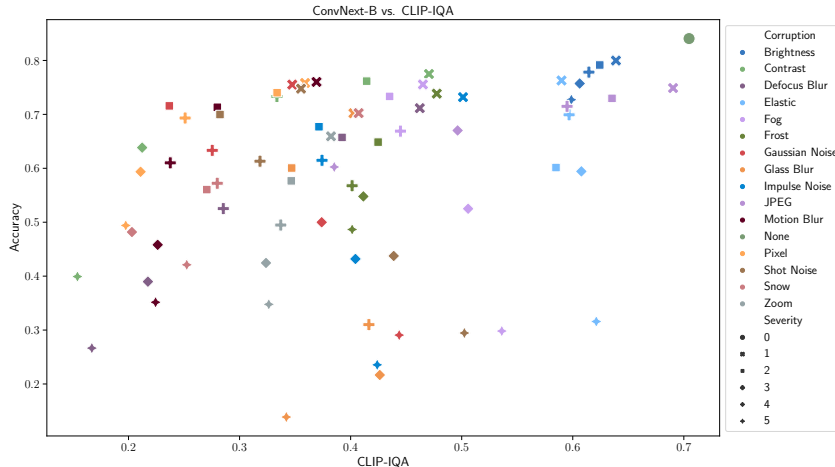


Figure 3: Accuracy (M) vs. IQ (Q) for ConvNext-B and CLIP-IQA respectively. Each point represents the average accuracy over all images in the ImageNet val set corrupted with the corresponding corruption/severity. Little correlation is observed between M , Q across all corruptions/severities and Q is weakly predictive of M .

Table 1: Correlation between IQ and accuracy, correctness. SRCC, PLCC computed using average accuracy for each (corruption, severity). AUC and CE based on point-wise predictions (95% CI within ± 0.001). SRCC, PLCC values have $p < 0.05$.

Model	IQA Metric	AUC \uparrow	CE \downarrow	$ KRCC \uparrow$	$ PLCC \uparrow$	$ SRCC \uparrow$
ConvNext-B	ARNIQA	0.517	0.677	0.088 ± 0.149	0.168 ± 0.215	0.127 ± 0.214
	BRISQUE	0.568	0.670	0.255 ± 0.129	0.398 ± 0.190	0.374 ± 0.182
	CLIP-IQA	0.567	0.670	0.273 ± 0.154	0.328 ± 0.202	0.378 ± 0.212
	TV	0.477	0.676	0.108 ± 0.183	0.138 ± 0.294	0.151 ± 0.255
ResNet34	ARNIQA	0.499	0.663	0.003 ± 0.155	0.006 ± 0.205	0.007 ± 0.225
	BRISQUE	0.552	0.658	0.175 ± 0.140	0.278 ± 0.186	0.254 ± 0.202
	CLIP-IQA	0.599	0.647	0.307 ± 0.159	0.467 ± 0.188	0.429 ± 0.207
	TV	0.500	0.657	0.051 ± 0.194	0.291 ± 0.256	0.047 ± 0.264
Swin-B	ARNIQA	0.510	0.675	0.069 ± 0.155	0.118 ± 0.230	0.098 ± 0.222
	BRISQUE	0.574	0.667	0.291 ± 0.131	0.443 ± 0.183	0.426 ± 0.178
	CLIP-IQA	0.571	0.667	0.290 ± 0.161	0.361 ± 0.199	0.410 ± 0.211
	TV	0.485	0.674	0.090 ± 0.180	0.153 ± 0.299	0.123 ± 0.255

when fixing Y , we find $mAUC = 0.5652$ ($\sigma = 0.08$) and $mCE = 0.6176$ ($\sigma = 0.1094$) suggesting that even when we control for Y , the predictability of DNN performance from the NR-IQA metrics remains weak.

These results suggest that NR-IQA metrics are likely sensitive to a different set of image features than task DNNs (i.e., no shared Z) and thus are barely, if at all, predictive of performance (i.e., they do not satisfy criterion **D3** from §3). The primary implication of this result is that if we intend to use IQ metrics to measure image quality/difficulty from the DNN perspective, common NR-IQ metrics may not be well-suited to this task and alternative approaches are needed.

5 RESTORING THE ASSOCIATION BETWEEN Q , M VIA STRONG TASK-GUIDANCE (**D3**)

The previous results indicated that existing NR-IQA meet **D1**, **D2**, **D4** but the lack of predictability (**D3**) between NR-IQA metrics and DNN accuracy/correctness is a major limitation in using these metrics for assessing dataset quality relative to potential downstream task models. Focusing specifically on **D3**, we next consider an alternative formulation of the causal model will allow us to recover a dependence between M , Q when conditioning on X .

Table 2: Correlation between IQ and accuracy, correctness. KRCC, SRCC, PLCC computed using average accuracy for each (corruption, severity). AUC and CE based on point-wise predictions (95% CI within ± 0.001). KRCC, SRCC, PLCC values have $p < 0.05$. Full table in Appendix E.

Model	IQA Metric	AUC \uparrow	CE \downarrow	$ KRCC \uparrow$	$ PLCC \uparrow$	$ SRCC \uparrow$
ConvNext-B	Q_h	0.772	0.562	0.660 ± 0.070	0.822 ± 0.070	0.854 ± 0.063
	Q_i	0.778	0.555	0.660 ± 0.067	0.826 ± 0.067	0.854 ± 0.063
	Q_p	0.826	0.504	0.738 ± 0.045	0.888 ± 0.045	0.910 ± 0.044
ResNet34	Q_h	0.848	0.470	0.862 ± 0.028	0.930 ± 0.028	0.969 ± 0.023
	Q_i	0.827	0.492	0.870 ± 0.015	0.951 ± 0.015	0.973 ± 0.020
	Q_p	0.850	0.461	0.886 ± 0.015	0.960 ± 0.015	0.977 ± 0.021
Swin-B	Q_h	0.766	0.578	0.532 ± 0.207	0.483 ± 0.207	0.654 ± 0.174
	Q_i	0.732	0.597	0.485 ± 0.203	0.458 ± 0.203	0.611 ± 0.181
	Q_p	0.807	0.529	0.603 ± 0.184	0.620 ± 0.184	0.732 ± 0.142

In the case where a pre-trained DNN f_θ is given, Figure 4 describes a scenario where the predictions from this DNN may also be used as indicators of quality. This parallels other work (Hendrycks et al., 2019) which shows that uncertainty in the output predictions is often a good predictor of the OOD nature of the input. Note here that while Q, M both depend on \hat{Y} , Q requires no knowledge of the labels. In this case, it is possible that \hat{Y} can be incorrect from the perspective of the ground truth label Y but still provide information about Q (e.g., via a low confidence prediction).

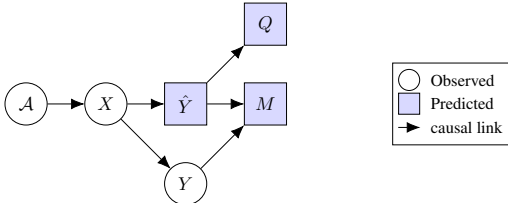


Figure 4: Causal diagram relating model accuracy (M) with IQ metrics (Q) with the additional dependence $\hat{Y} \rightarrow Q$.

Because this approach uses a model for Q that is already trained for the classification task, we consider this **strong** task-guided IQA (TG-IQA). Clearly, this provides an alternative to the conventional NR-IQA metrics but now violates **D4** since Q is informed directly by the same model trained for the task and measured by M . Nonetheless, our (temporary) goal here is to use the causal framework to show there exists a case where Q, M are associated through a common set of features Z . Our hypothesis is that with **strong** TG-IQA we should observe a clear correlation between M, Q .

We examine the case where Q is determined directly from predictions generated by a pre-trained task DNN. In this case, let f_θ be pre-trained to predict $P(Y|X)$. Then, let $z \in \mathbb{R}^k$ be the pre-softmax logits obtained from f_θ and $\hat{y} = \text{softmax}(z)$ where each $\hat{y}_i = P(Y = i|X)$ for $i \in 1, \dots, K$. We consider three possible variants of Q in this setting: (1) Max probability: $Q_p := \max_i \hat{y}_i$, (2) Entropy: $Q_h := H(\hat{y}) = -\sum_i \hat{y}_i \log \hat{y}_i$, and (3) Max logit: $Q_l := \max_i z_i$. While all three cases are inherently tied to the underlying label set \mathcal{Y} , the values of Q do **not** have access to the ground truth label Y . Each of these Q implicitly capture a DNN’s confidence about its prediction and the natural underlying hypothesis is that confidence and image quality are positively correlated (i.e., as quality decreases, confidence also tends to decrease). These choices for Q are driven by their use in out-of-distribution (Hendrycks & Gimpel, 2016; Hendrycks et al., 2019; 2020) and distribution shift detection (Wang et al., 2020).

5.1 EXPERIMENT - STRONG TASK-GUIDED IQA

Using the same setup as in Section 4.1, we now replace the NR-IQA metrics with Q_p, Q_h, Q_l . As in Section 4.2, we examine the group-wise correlation and point-wise predictability of M from Q . To ensure our test of predictability is fair, we use separate models for obtaining M and Q (namely, ConvNext-B and Swin-B respectively). We provide additional results for other model pairs in Appendix E. Figure 5 shows the group-wise relationship between Q, M where groups are averages over all images for the corresponding corruption, severity.

The results in Figure 5 and Table 2 show that strong task-guidance for Q results in high correlation between Q, M and predictability of M from Q (**D3**). This result, while expected, is important to show that using the causal framework it is possible to find a metric Q that relies on a similar set of

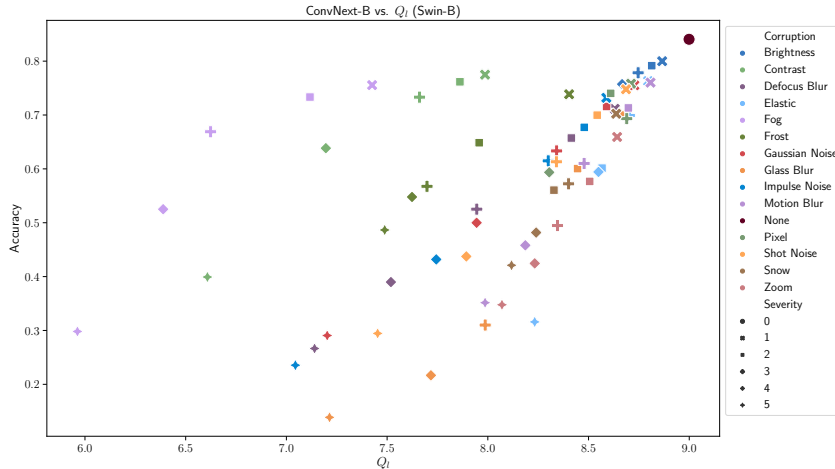


Figure 5: Accuracy vs. max logit using ConvNext-B for the task model and Swin-B for Q_l which generally outperforms the other variants

features as separate task models. However, like the previous section, this approach is only a partial solution as it satisfies **D1**, **D2**, **D3** but clearly violates **D4** by requiring a model already trained for the classification task.

6 RESTORING THE ASSOCIATION BETWEEN Q , M VIA WEAK TASK-GUIDANCE (**D3**, **D4**)

So far, §4 showed that common NR-IQA metrics are weakly predictive of DNN performance and are therefore not viable candidates for supporting image/dataset-level analysis given our desiderata (§3). Then, we were able to address the predictability issue (**D3**) in §5 using strong task-guidance, but at the cost of requiring a task model already trained for the classification task (a violation of **D4**).

To address the aforementioned issues, we consider instead a weaker form of task-guidance where quality metrics can be aligned with task-specific information without requiring the expense of training a new task model directly on the dataset of interest (**D4**). In this setting shown in Figure 6, the computation of Q is dependent not only on the image X but on the label set \mathcal{Y} . The task T is used as a selection variable (Zadrozny, 2004; Bareinboim et al., 2022) on which the dataset is conditioned, and as a collider in the DAG, T creates an association between M , Q .

6.1 ZERO-SHOT CLIP IQA

We propose a quality metric that uses Zero-Shot (ZS) capabilities of the multi-modal CLIP foundation model (Radford et al., 2021) in order to address all desiderata (§3). In particular, we derive a new image quality metric (ZSCLIP-IQA) based on a zero-shot classification problem for our data and task of interest.

Let $\mathcal{D} = \{(x_i, y_i)\}_{i=1}^N$ be our dataset with images x and labels y , $f : \mathcal{X} \rightarrow \mathcal{Z}$ be our CLIP image embedding network ($\mathcal{Z} \in \mathbb{R}^d$), and $g : \mathcal{T} \rightarrow \mathcal{W}$ be our CLIP text/token-embedding network ($\mathcal{W} \in \mathbb{R}^d$).

We define a set of task-relevant classes/tokens $\mathcal{T} = \{T_i\}_{i=1}^K$ that capture the text labels for concepts or entities likely to occur in the images (e.g., $K = 1000$ classes in the ImageNet dataset). We embed each of the text tokens $g(T_i) = w_i$ and normalize to get a unit vector representation for each token. Note when using CLIP as our text embedding network, we may

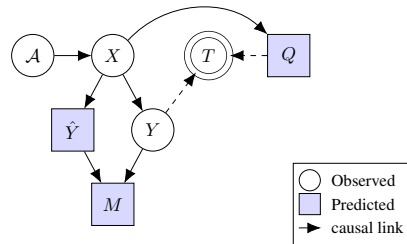


Figure 6: Causal DAG relating model performance (M) with IQ metrics (Q). Q uses information about the label set \mathcal{Y} . The task T is viewed as a selection variable which influences both the labels Y and Q .

Table 3: Correlation between IQ and accuracy. KRCC, SRCC, PLCC based on average accuracy for each (corruption, severity) combination. AUC and CE are computed based on point-wise predictions and all have 95% CI within ± 0.001 . All KRCC, SRCC, PLCC values have $p < 0.005$.

Model	ZSCLIP-IQA	AUC \uparrow	CE \downarrow	$ KRCC \uparrow$	$ PLCC \uparrow$	$ SRCC \uparrow$
ConvNext-B	Q_h	0.349	0.677	0.738 ± 0.067	0.869 ± 0.059	0.906 ± 0.048
	Q_l	0.675	0.632	0.573 ± 0.084	0.764 ± 0.080	0.783 ± 0.085
	Q_p	0.602	0.677	0.788 ± 0.056	0.884 ± 0.048	0.937 ± 0.034
ResNet34	Q_h	0.666	0.663	0.800 ± 0.059	0.936 ± 0.028	0.945 ± 0.032
	Q_l	0.692	0.609	0.630 ± 0.087	0.814 ± 0.055	0.820 ± 0.084
	Q_p	0.368	0.663	0.834 ± 0.049	0.949 ± 0.024	0.959 ± 0.026
Swin-B	Q_h	0.354	0.676	0.735 ± 0.072	0.864 ± 0.063	0.904 ± 0.054
	Q_l	0.672	0.633	0.538 ± 0.094	0.718 ± 0.096	0.743 ± 0.098
	Q_p	0.601	0.676	0.778 ± 0.059	0.879 ± 0.050	0.935 ± 0.034

also augment T_i to include additional words (e.g., "A picture of a <token>"). The full set $\mathbf{W} = [w_0; w_1; \dots w_K] \in \mathbb{R}^{d \times K}$ constitutes the ZS weights.

To evaluate image quality, we compute image embeddings $f_\theta(x) = z$ for $x \in \mathcal{D}$ which we normalize to be unit length. For each image, we compute the cosine similarity between the image embedding and each of the tokens $s = z\mathbf{W}$ (with $z \in \mathbb{R}^d$, $s \in \mathbb{R}^K$) and compute estimated class probabilities via a softmax over similarity scores ($\hat{y} = \text{softmax}(s)$). As in the strong TG-IQA scenario, we implement three variants of Q : (1) Max probability: $Q_p := \max_i \hat{y}_i$, (2) Entropy: $Q_h := H(\hat{y}) = -\sum_i \hat{y}_i \log \hat{y}_i$, and (3) Max-logit: $Q_l := \max_i s_i$.

6.2 EXPERIMENT - WEAK TASK-GUIDED IQA

Using the setup from §4 we now replace the NR-IQA metrics with Q_p, Q_h, Q_l based on the ZSCLIP-IQA method described above. We again examine the group-wise correlation and point-wise predictability of M from Q . Figure 7 and Table 3 show that weak task-guidance is enough to restore the association between Q and M without requiring a new task model to be trained on the dataset of interest.

Remark: While the CLIP backbone is pre-trained on a self-supervised task that resembles classification, it was not exposed to ImageNet (or IN-C) data during its training (see §5 in (Radford et al., 2021)) and can be effectively used here in a zero-shot setting to satisfy **D4**. In fact, while methods like CLIP-IQA and ARNIQA also rely on pre-trained backbones, the results of Tables 1 and 3 show that only ZSCLIP-IQA is “guided” (via our causal framework) to be a stronger predictor of DNN performance compared to other methods calibrated to human perceptual judgment.

6.3 EXPERIMENT - PREDICTABILITY OF DNN PERFORMANCE FOR MILDLY CORRUPTED DATASETS

In the previous experiments, the use of IN-C allowed us to investigate the large-scale effect of image corruptions on the predictability of performance by using multiple corrupted versions of the validation set with multiple levels of severity. In real-world datasets, we expect that only a small fraction of images will be corrupted. We next examine the extent to which IQA metrics can be used to show differences between the quality distributions of datasets containing varying levels of corruption while still satisfying **D1-D4** in these more realistic settings.

To answer this question, we generate new variants of IN-val consisting of mixtures of clean and corrupted images. For each variant, we specify a set of valid corruptions \mathcal{C} , severities \mathcal{S} , and a corruption probability p_c . We choose a fraction $1 - p_c$ of the original IN-val image IDs to remain as clean images and a fraction p_c to be corrupted. The corrupted images are sampled uniformly amongst the corruptions $c \in \mathcal{C}$ and severities $s \in \mathcal{S}$. The resulting variant consists of the original 50k image IDs with a mixture of clean and corrupted images.

We choose \mathcal{C} to consist of all 15 corruptions in the IN-C dataset and limit severity to $\mathcal{S} = \{1, 2, 3\}$ in order to further test the sensitivity of the IQA metrics (**D1**). We create variants of the IN-val dataset for $p_c = N/100$ for $N \in [1, \dots, 20]$. We evaluate the DNNs on these dataset variants and estimate predictability using logistic regression as in previous experiments. We compute $mAUC$ over all p_c

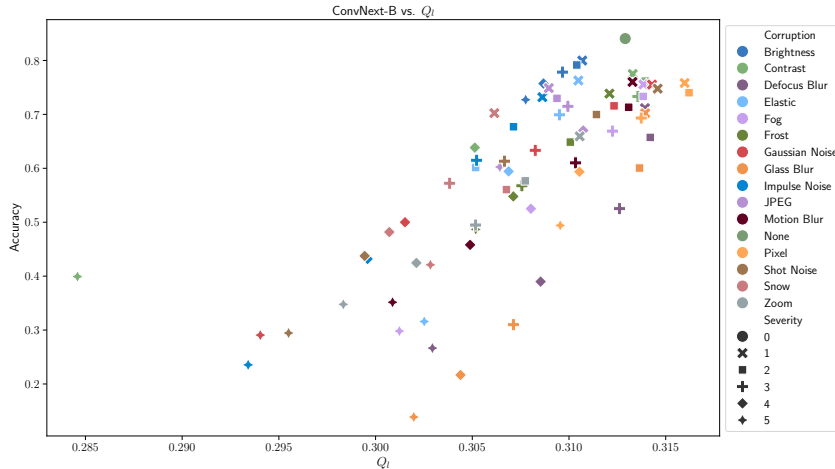


Figure 7: Accuracy vs. IQ with ConvNext-B as the task model M and ZSCLIP-IQA max-logit as the quality metric Q_l which generally outperforms the other variants.

variants and find ZSCLIP-IQA (Q_l) outperforms all other NR-IQA metrics with $mAUC = 0.64$ with the next best (CLIP-IQA) achieving only $mAUC = 0.57$. The results show that while all metrics can distinguish between differences in the quality distributions of the dataset variants, only ZSCLIP-IQA achieves high predictability over all variants. Conventional IQA metrics improve only as the number of distorted images in the dataset increases (where it becomes easier to separate clean and corrupted images). The full results are found in Appendix H and show that predictability with ZSCLIP-IQA is stable with respect to changes in the proportion of clean/corrupted images in the dataset whereas more traditional NR-IQA metrics remain near random chance AUC and exhibit higher variance as p_c changes.

7 DISCUSSION

In this work, we were motivated to identify measures of image quality that allow us to produce IQ-driven priors on DNN performance. We presented a causal inference framework for this problem and proposed a set of IQ metric desiderata to guide our analysis. Using our causal framework, we show conditions where image quality measures can be predictive of DNN performance. We then provide a detailed examination of the relationship between conventional NR-IQA metrics and DNN performance. We use our causal framework and extensive empirical evaluations in the context of image classification to demonstrate that common NR-IQA do not satisfy our desired IQ criteria. We then use the causal approach to develop the task-guided ZSCLIP-IQA metric that provides a causality-driven proof-of-concept metric that satisfies all IQ desiderata and paves the way for future research to improve the alignment between IQA metrics and DNN performance.

Potential negative societal impacts As a tool for analysis, the proposed causal framework poses minimal societal risks. While causal models require assumptions about the data generating process, these assumptions are made explicitly in the causal graph and improve the overall transparency of the analysis. Of greater concern is the possibility that using quality metrics to prune/resample datasets may lead to unintended consequences such as removing poor-quality images in a way that disparately affects protected groups. While our work does not address the question of dataset pruning/resampling, we mention this to help ensure that future researchers consider these possibilities in their own work.

Limitations and future work We first recognize that image quality alone is insufficient to predict task model performance as both image content and composition play a role in task difficulty and the relationship between IQA and performance may be confounded by other factors. Nonetheless, we show that our causal framework still allows us to analyze the conditions where quality properties of our dataset may be correlated with DNN performance. Our ZSCLIP-IQA method provides one solution that satisfies the proposed IQ desiderata but we believe there are many opportunities for improving on this approach in future research.

We also acknowledge that our experiments only addressed image classification tasks. We focused initially on classification since it is well-studied and clearly defined, with many public benchmarks available for evaluation. Even in this context, we are the first to show that the notion of quality is task-dependent (i.e., perceptual judgment vs. classification). Our primary contribution in this work is the causal framework and we believe this provides a strong foundation for supporting future research that examines similar questions for a wider range of vision tasks.

REFERENCES

- Amro Abbas, Evgenia Rusak, Kushal Tirumala, Wieland Brendel, Kamalika Chaudhuri, and Ari S Morcos. Effective pruning of web-scale datasets based on complexity of concept clusters. January 2024.
- Lorenzo Agnolucci, Leonardo Galteri, Marco Bertini, and Alberto Del Bimbo. Arniqa: Learning distortion manifold for image quality assessment. In *Proceedings of the IEEE/CVF Winter Conference on Applications of Computer Vision*, pp. 189–198, 2024.
- Elias Bareinboim, Jin Tian, and Judea Pearl. Recovering from selection bias in causal and statistical inference. In *Probabilistic and Causal Inference*, pp. 433–450. ACM, New York, NY, USA, February 2022.
- Alexander Brown, Nenad Tomasev, Jan Freyberg, Yuan Liu, Alan Karthikesalingam, and Jessica Schrouff. Detecting shortcut learning for fair medical AI using shortcut testing. (1):4314, July 2023.
- Vincent S Chen, Sen Wu, Zhenzhen Weng, Alexander Ratner, and Christopher Ré. Slice-based learning: A programming model for residual learning in critical data slices. *Adv. Neural Inf. Process. Syst.*, 32:9392–9402, December 2019.
- Yeounoh Chung, Tim Kraska, Neoklis Polyzotis, Ki Hyun Tae, and Steven Euijong Whang. Slice finder: Automated data slicing for model validation. In *2019 IEEE 35th International Conference on Data Engineering (ICDE)*, pp. 1550–1553. IEEE, April 2019.
- Josip Djolonga, Jessica Yung, Michael Tschannen, Rob Romijnders, Lucas Beyer, Alexander Kolesnikov, Joan Puigcerver, Matthias Minderer, Alexander Nicholas D’Amour, Dan Moldovan, Sylvain Gelly, Neil Houlsby, Xiaohua Zhai, and Mario Lučić. On robustness and transferability of convolutional neural networks. In *Conference on Computer Vision and Pattern Recognition*, 2021.
- Nathan Drenkow and Mathias Unberath. RobustCLEVR: A benchmark and framework for evaluating robustness in object-centric learning. August 2023.
- Sabri Eyuboglu, Maya Varma, Khaled Saab, Jean-Benoit Delbrouck, Christopher Lee-Messer, Jared Dunmon, James Zou, and Christopher Ré. Domino: Discovering systematic errors with cross-modal embeddings. March 2022.
- Robert Geirhos, Patricia Rubisch, Claudio Michaelis, Matthias Bethge, Felix A Wichmann, and Wieland Brendel. ImageNet-trained CNNs are biased towards texture; increasing shape bias improves accuracy and robustness. November 2018.
- Robert Geirhos, Jörn-Henrik Jacobsen, Claudio Michaelis, Richard Zemel, Wieland Brendel, Matthias Bethge, and Felix A Wichmann. Shortcut learning in deep neural networks. *Nature Machine Intelligence*, 2(11): 665–673, November 2020.
- Robert Geirhos, Kantharaju Narayanappa, Benjamin Mitzkus, Tizian Thieringer, Matthias Bethge, Felix A Wichmann, and Wieland Brendel. Partial success in closing the gap between human and machine vision. *arXiv preprint arXiv:2106.07411*, 2021.
- Kaiming He, Xiangyu Zhang, Shaoqing Ren, and Jian Sun. Deep residual learning for image recognition. In *Proceedings of the IEEE conference on computer vision and pattern recognition*, pp. 770–778, 2016.
- Muyang He, Shuo Yang, Tiejun Huang, and Bo Zhao. Large-scale dataset pruning with dynamic uncertainty. June 2023.
- Dan Hendrycks and Thomas Dietterich. Benchmarking neural network robustness to common corruptions and perturbations. pp. –, University of California, Berkeley, United States Oregon State University, United States, March 2019. International Conference on Learning Representations, ICLR.
- Dan Hendrycks and Kevin Gimpel. A baseline for detecting misclassified and Out-of-Distribution examples in neural networks. October 2016.

- Dan Hendrycks, Steven Basart, Mantas Mazeika, Andy Zou, Joe Kwon, Mohammadreza Mostajabi, Jacob Steinhardt, and Dawn Song. Scaling Out-of-Distribution detection for Real-World settings. November 2019.
- Dan Hendrycks, Steven Basart, Norman Mu, Saurav Kadavath, Frank Wang, Evan Dorundo, Rahul Desai, Tyler Zhu, Samyak Parajuli, Mike Guo, and Others. The many faces of robustness: A critical analysis of out-of-distribution generalization. *arXiv preprint arXiv:2006.16241*, 2020.
- Katherine L Hermann, Ting Chen, and Simon Kornblith. The origins and prevalence of texture bias in convolutional neural networks. November 2019.
- Mark Ibrahim, Quentin Garrido, Ari Morcos, and Diane Bouchacourt. The robustness limits of SoTA vision models to natural variation. October 2022.
- Andrew Ilyas, Sung Min Park, Logan Engstrom, Guillaume Leclerc, and Aleksander Madry. Datamodels: Predicting predictions from training data. February 2022.
- Devin Kwok, Nikhil Anand, Jonathan Frankle, Gintare Karolina Dziugaite, and David Rolnick. Dataset difficulty and the role of inductive bias. January 2024.
- Jinkun Lin, Anqi Zhang, Mathias Lécuyer, Jinyang Li, Aurojit Panda, and Siddhartha Sen. Measuring the effect of training data on deep learning predictions via randomized experiments. In Kamalika Chaudhuri, Stefanie Jegelka, Le Song, Csaba Szepesvari, Gang Niu, and Sivan Sabato (eds.), *Proceedings of the 39th International Conference on Machine Learning*, volume 162 of *Proceedings of Machine Learning Research*, pp. 13468–13504. PMLR, 2022.
- Ze Liu, Yutong Lin, Yue Cao, Han Hu, Yixuan Wei, Zheng Zhang, Stephen Lin, and Baining Guo. Swin transformer: Hierarchical vision transformer using shifted windows. pp. 10012–10022, March 2021.
- Zhuang Liu, Hanzi Mao, Chao-Yuan Wu, Christoph Feichtenhofer, Trevor Darrell, and Saining Xie. A ConvNet for the 2020s. January 2022.
- Kede Ma, Wentao Liu, Kai Zhang, Zhengfang Duanmu, Zhou Wang, and Wangmeng Zuo. End-to-End blind image quality assessment using deep neural networks. *IEEE Trans. Image Process.*, 27(3):1202–1213, March 2018.
- Sébastien Marcel and Yann Rodriguez. Torchvision the machine-vision package of torch. In *Proceedings of the 18th ACM international conference on Multimedia*, MM '10, pp. 1485–1488, New York, NY, USA, October 2010. Association for Computing Machinery.
- Anish Mittal, Anush Krishna Moorthy, and Alan Conrad Bovik. No-reference image quality assessment in the spatial domain. *IEEE Transactions on image processing*, 21(12):4695–4708, 2012.
- Cathy Ong Ly, Balagopal Unnikrishnan, Tony Tadic, Tirth Patel, Joe Duhamel, Sonja Kandel, Yasbanoo Moayedi, Michael Brudno, Andrew Hope, Heather Ross, and Chris McIntosh. Shortcut learning in medical AI hinders generalization: method for estimating AI model generalization without external data. *npj Digital Medicine*, 7(1):1–10, May 2024.
- Mitchell Pavlak, Nathan Drenkow, Nicholas Petrick, Mohammad Mehdi Farhangi, and Mathias Unberath. Data AUDIT: Identifying attribute utility- and Detectability-Induced bias in task models. April 2023.
- Alec Radford, Jong Wook Kim, Chris Hallacy, Aditya Ramesh, Gabriel Goh, Sandhini Agarwal, Girish Sastry, Amanda Askell, Pamela Mishkin, Jack Clark, Gretchen Krueger, and Ilya Sutskever. Learning transferable visual models from natural language supervision. February 2021.
- Christoph Schuhmann, Romain Beaumont, Richard Vencu, Cade Gordon, Ross Wightman, Mehdi Cherti, Theo Coombes, Aarush Katta, Clayton Mullis, Mitchell Wortsman, P Schramowski, Srivatsa Kundurthy, Katherine Crowson, Ludwig Schmidt, R Kaczmarczyk, and J Jitsev. LAION-5B: An open large-scale dataset for training next generation image-text models. *Adv. Neural Inf. Process. Syst.*, abs/2210.08402, October 2022.
- N Sohoni, Jared A Dunnmon, Geoffrey Angus, Albert Gu, and C Ré. No subclass left behind: Fine-grained robustness in coarse-grained classification problems. *Adv. Neural Inf. Process. Syst.*, abs/2011.12945, November 2020.
- Chen Sun, Abhinav Shrivastava, Saurabh Singh, and A Gupta. Revisiting unreasonable effectiveness of data in deep learning era. *ICCV*, pp. 843–852, July 2017.
- Haoru Tan, Sitong Wu, Fei Du, Yukang Chen, Zhibin Wang, Fan Wang, and Xiaojuan Qi. Data pruning via Moving-one-Sample-out. October 2023.

Rohan Taori, Achal Dave, Vaishal Shankar, Nicholas Carlini, Benjamin Recht, and Ludwig Schmidt. Measuring robustness to natural distribution shifts in image classification. In H Larochelle, M Ranzato, R Hadsell, M F Balcan, and H Lin (eds.), *Advances in Neural Information Processing Systems*, volume 33, pp. 18583–18599. Curran Associates, Inc., 2020.

Dequan Wang, Evan Shelhamer, Shaoteng Liu, Bruno Olshausen, and Trevor Darrell. Tent: Fully test-time adaptation by entropy minimization. June 2020.

Jianyi Wang, Kelvin C K Chan, and Chen Change Loy. Exploring CLIP for assessing the look and feel of images. *National Conference on Artificial Intelligence*, pp. 2555–2563, July 2022.

Zhou Wang. Image quality assessment: from error visibility to structural similarity. *IEEE transactions on image processing*, 13(4):600–612, 2004.

Zhou Wang and Alan C Bovik. *Modern Image Quality Assessment*. Springer International Publishing.

Felix A Wichmann and Robert Geirhos. Are deep neural networks adequate behavioral models of human visual perception? *Annu Rev Vis Sci*, 9:501–524, September 2023.

Shaoping Xu, Shunliang Jiang, and Weidong Min. No-reference/Blind image quality assessment: A survey. *IETE Tech. Rev.*, 34(3):223–245, May 2017.

Bianca Zadrozny. Learning and evaluating classifiers under sample selection bias. In *Twenty-first international conference on Machine learning - ICML '04*, New York, New York, USA, 2004. ACM Press.

John R Zech, Marcus A Badgeley, Manway Liu, Anthony B Costa, Joseph J Titano, and Eric Karl Oermann. Variable generalization performance of a deep learning model to detect pneumonia in chest radiographs: A cross-sectional study. *PLoS Med.*, 15(11):e1002683, November 2018.

Lin Zhang, Lei Zhang, Xuanqin Mou, and David Zhang. Fsim: A feature similarity index for image quality assessment. *IEEE transactions on Image Processing*, 20(8):2378–2386, 2011.

Richard Zhang, Phillip Isola, Alexei A Efros, Eli Shechtman, and Oliver Wang. The unreasonable effectiveness of deep features as a perceptual metric. In *Proceedings of the IEEE conference on computer vision and pattern recognition*, pp. 586–595, 2018.

A CAUSAL MODEL FOR NR-/FR-IQA

We provide here the causal models for the NR-IQA and FR-IQA settings in Figure 8.

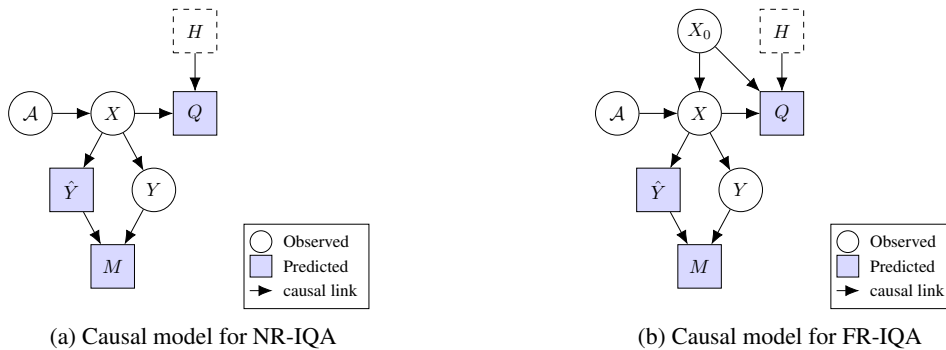


Figure 8: Causal model for the NR-/FR-IQA settings. The FR-IQA setting includes X_0 which is the reference image. In both models, H indicates human annotator guidance which reflects that IQ metrics are typically calibrated against human perceptual judgements (dashed-line box indicates H is not used directly in the calculation of Q).

While the main manuscript focused on the NR-IQA setting, we can see from the causal models here that the results generalize to the FR-IQA case as well. In particular, the independence of Q , M given X is not affected by whether a “clean” reference image (X_0) is available for computing Q . Also, these models also account for the influence of human annotators H in calibrating the function for computing Q , but not that this does not change the relationship between M , Q .

B CAUSAL MODEL FOR IQA WITH LATENT FEATURES

In understanding the difference between the baseline IQA formulation in Figure 1 and the shared features formulation of Figure 2 in Section 3, we provide an expanded version of the baseline DAG in Figure 9. Here we show that the task DNN for computing \hat{Y} and the function for computing Q rely on latent features $Z_{\hat{Y}}$ and Z_Q respectively.

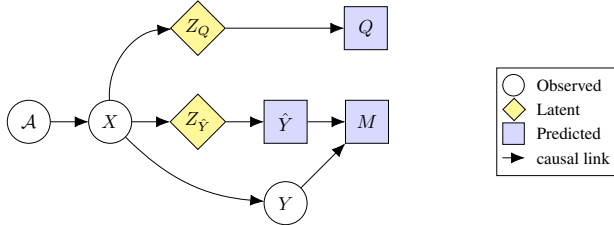


Figure 9: Causal model for IQA that accounts for the use of latent features by the task DNN and IQ metric towards computing M and Q respectively.

In this expanded model, $Z_{\hat{Y}}$ and Z_Q are independent given X and not “shared”, and therefore $Q \perp M \mid X$ as discussed in §3. In contrast, Figure 2 considers the case where Z represents the features derived from X that are common between $Z_{\hat{Y}}$ and Z_Q shown in the baseline case above. Thus, Figure 2 shows the case where X does not block all paths between Q, M since a path exists from Q to M through Z . This ensures that Q and M will be correlated given X unlike in the baseline case above.

C CAUSAL MODEL FOR COMMON CORRUPTIONS ROBUSTNESS EVALUATION

The common corruptions framework (Hendrycks & Dietterich, 2019) is used in our experiments to ensure full control of the image distortion types and severity. Figure 10 shows a version of the baseline IQA causal model customized to account for the corruption process used by this evaluation framework. Here, the corrupted image X is determined by the corruption function (e.g., Gaussian noise, defocus blur, fog, contrast, brightness, JPEG compression), the severity ($S \in \{1, 2, 3, 4, 5\}$), and the “clean” image X_0 .

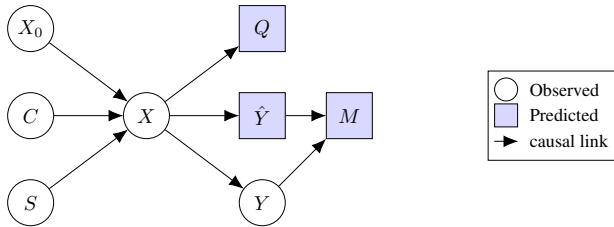


Figure 10: Causal model for the common corruptions framework where C refers to the corruption type, S refers to the corruption severity, and X_0 is the unperturbed, “clean” image.

In this setting, we see that C, S replace the original set of imaging factors \mathcal{A} in the graph in Figure 1. As such, the analysis from §3 holds in the common corruptions framework and allows us to study the relationship between Q, M in a setting where we can precisely control the imaging conditions.

D RELATIONSHIP OF NR-IQA AND DNN PERFORMANCE METRICS

In Figures 11, 12, and 13 we show the relationship of additional NR-IQA metrics with DNN performance for additional architectures and metrics. In general, we see weak trends in accuracy vs. average IQ suggesting that these metrics are most consistent with the causal model in Figure 1.

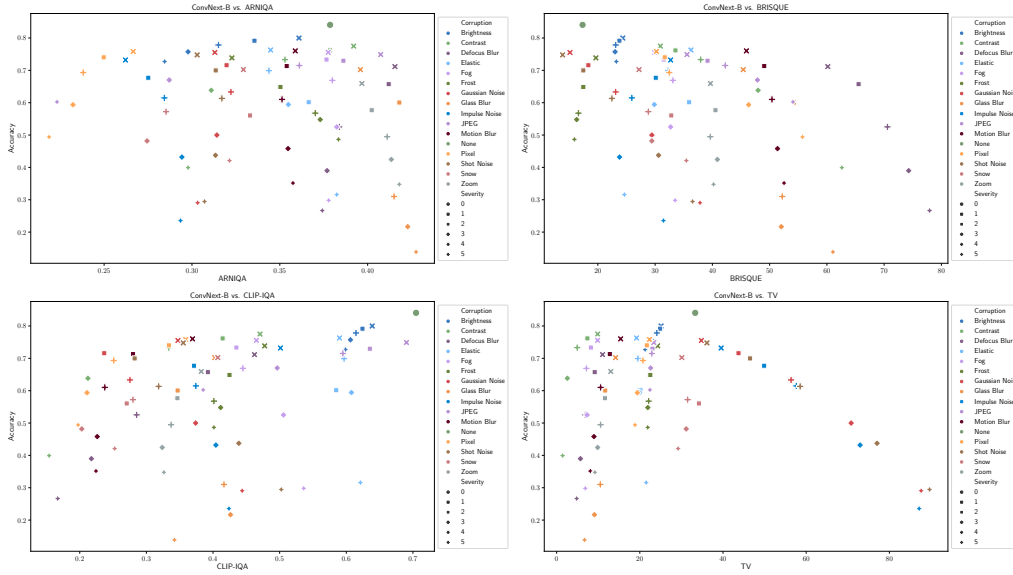


Figure 11: Comparison of ConvNext-B accuracy with (clockwise) ARNIQA, BRISQUE, CLIP-IQA, and TV. Little correlation is observed between group-wise accuracy and each NR-IQA metric.

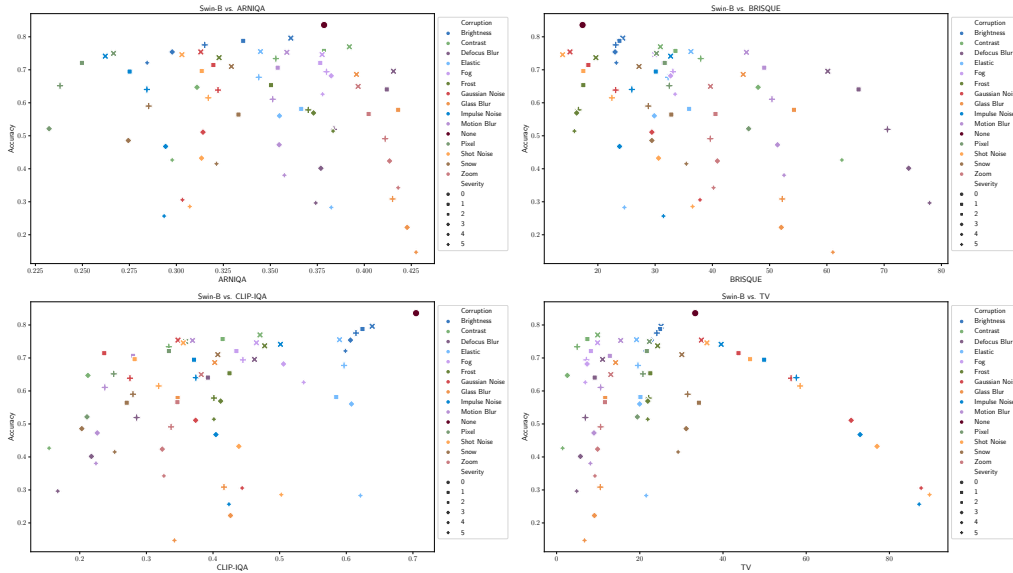


Figure 12: Comparison of Swin-B accuracy with (clockwise) ARNIQA, BRISQUE, CLIP-IQA, and TV. Little correlation is observed between group-wise accuracy and each NR-IQA metric.

E RELATIONSHIP OF STRONG TASK-GUIDED IQA AND DNN PERFORMANCE METRICS

In Figures 14, 15, 16, we examine the relationship between DNN performance and the strong task-guided metrics (Q_p , Q_h , Q_l) described in §5. Each figure pairs the task DNN under consideration with a pre-trained task model used to compute the quality metric.

Table 4 also shows the point-wise predictability results for the strong task-guided IQA case. This table extends Table 2 for additional task DNNs. Results here show that strong task-guided IQA metrics are highly correlated with DNN performance and that predictability remains high regardless of whether the pre-trained DNN used to compute Q is the same DNN used to obtain M .

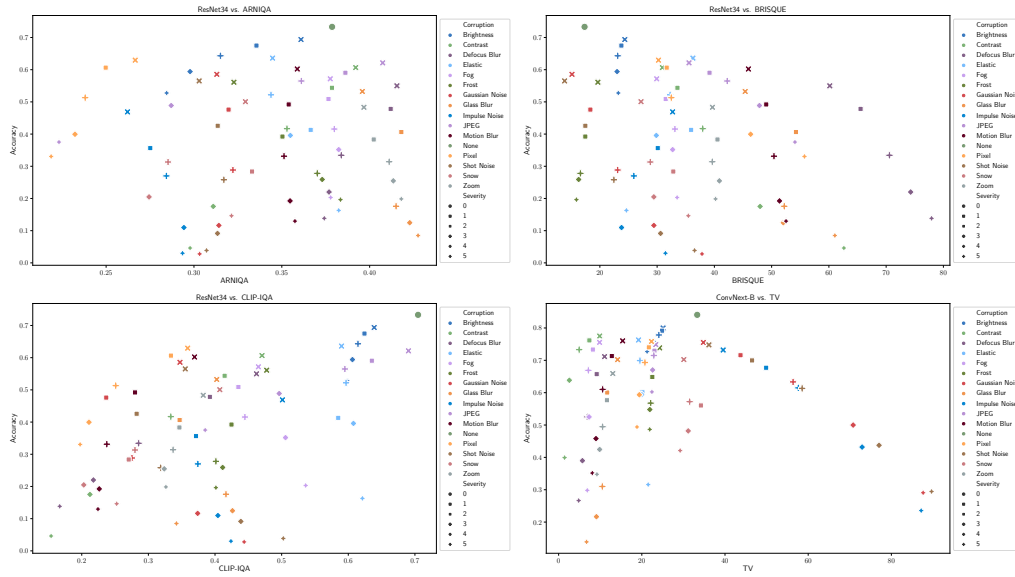


Figure 13: Comparison of ResNet34 accuracy with (clockwise) ARNIQA, BRISQUE, CLIP-IQA, and TV. Little correlation is observed between group-wise accuracy and each NR-IQA metric.

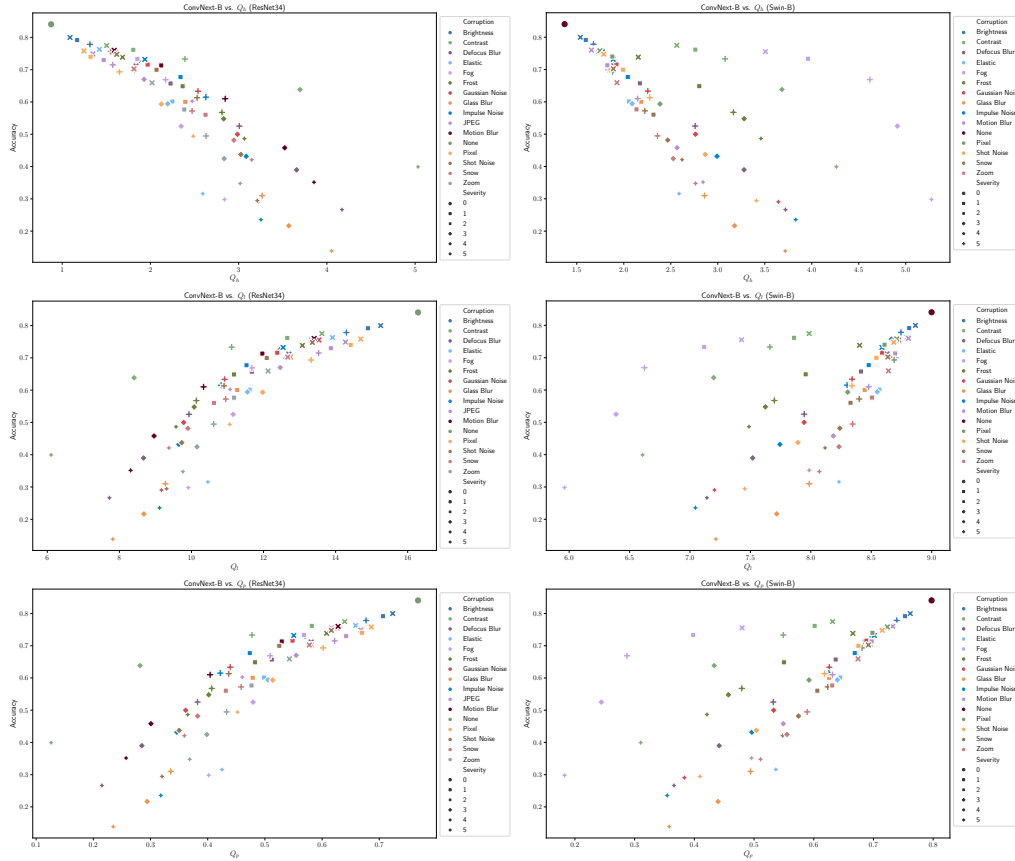


Figure 14: Comparison of ConvNext-B accuracy with (row) Q_h , Q_l , Q_p computed using (col) ResNet34, Swin-B. High correlation is observed between each IQA metric and accuracy.

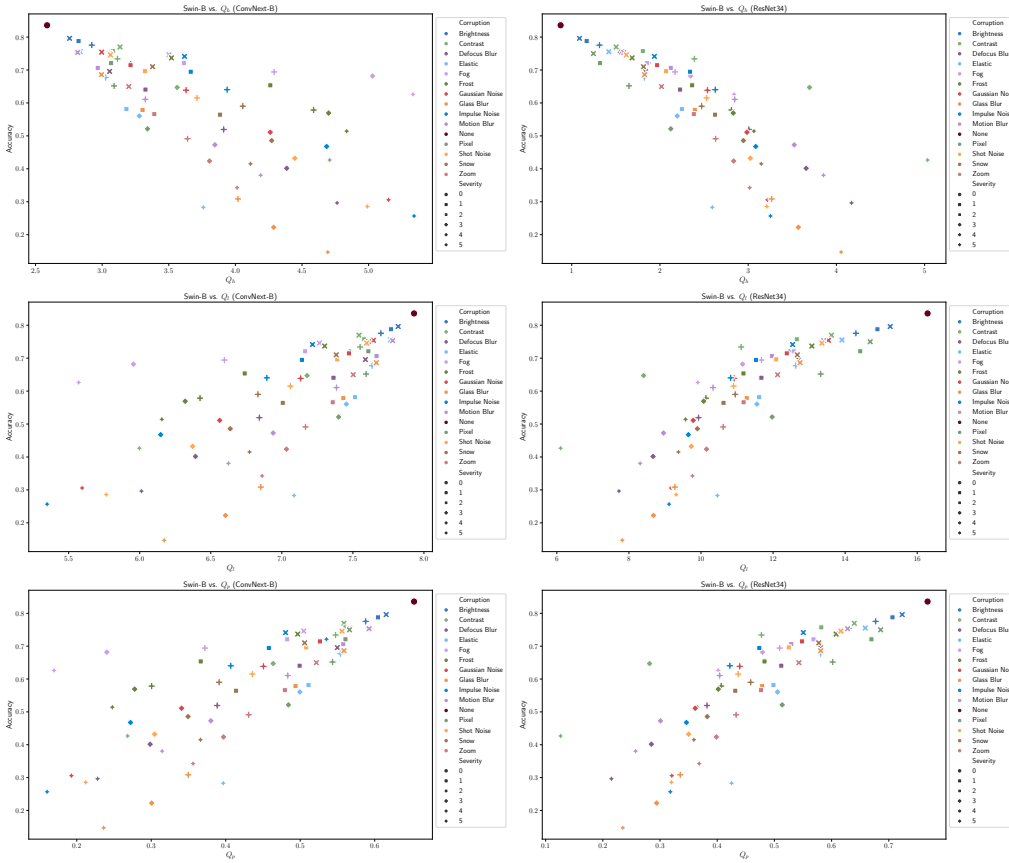


Figure 15: Comparison of Swin-B accuracy with (row) Q_h , Q_l , Q_p computed using (col) ConvNext-B, ResNet34. High correlation is observed between each IQA metric and accuracy.

F RELATIONSHIP OF WEAK TASK-GUIDED IQA AND DNN PERFORMANCE METRICS

We provide Figures 17, 18, 19 showing the relationship between DNN performance the weak task-guided ZSCLIP-IQA metric from §6.

G CONTROLLING FOR IMAGE CONTENT WHEN EVALUATING PREDICTABILITY

The experiments of §4-6 examined predictability by modeling $P(M|Q, X)$. Since the content of X may be a confounder for both M, Q , we attempt to control for it in two ways.

In the first case, we take advantage of the synthetic nature of the IN-C dataset by looking at the predictability of M from Q for each image in the dataset separately which allows us to control the content precisely and only change the quality characteristics. For this experiment, we train a logistic regression classifier to predict $P(M|Q)$ for individual image IDs trained using only M, Q computed from the set of distorted variants of each specific image ID. Given the original clean image and 15 corruptions with 5 severity levels each, we run 5-fold cross-validation with an 80/20 train/test split of the 76 total images. We repeat this for all 50k image IDs in the ImageNet validation set. The results shown in Figure 20a are an average of the AUC over all image IDs and folds.

We see that even when controlling for the image content the weak task-guided IQA generally achieves the highest $mAUC$ with the lowest variance. Overall, this supports our hypothesis and causal analysis that weak task-guidance provides a means to associate M, Q even when conditioning on the image directly.

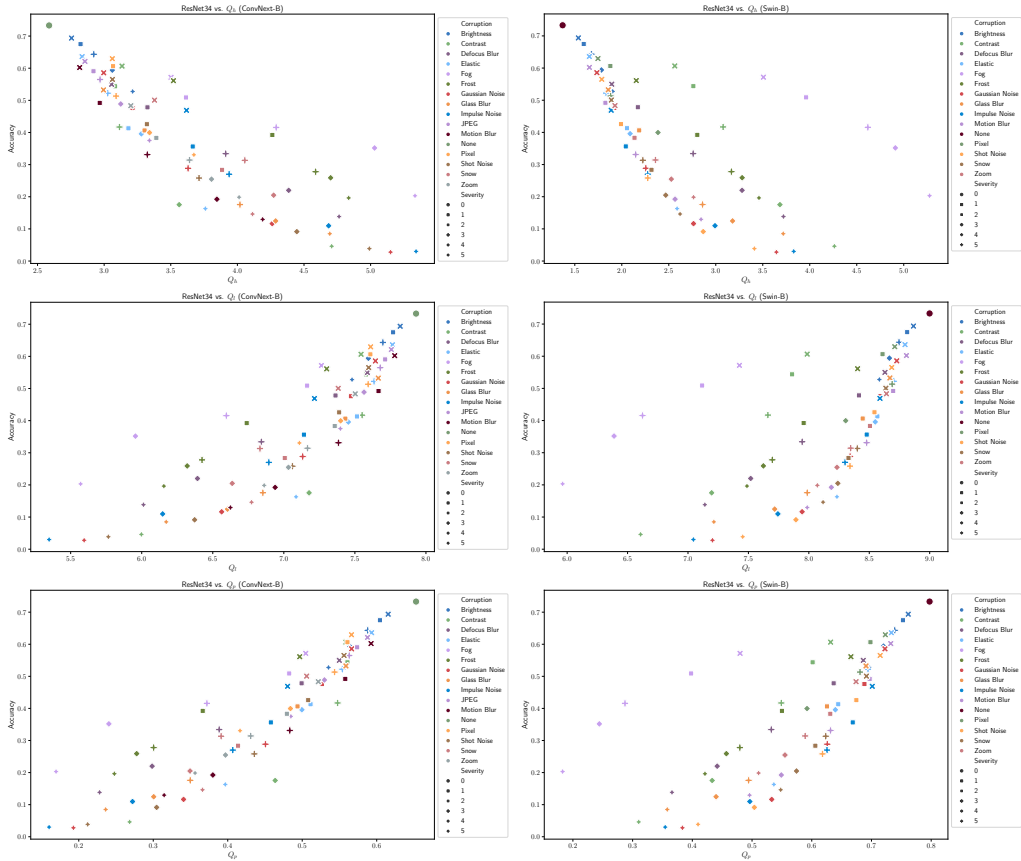


Figure 16: Comparison of ResNet34 accuracy with (row) Q_h, Q_l, Q_p computed using (col) ConvNext-B, Swin-B. High correlation is observed between each IQA metric and accuracy.

In the second case, we adjust for image content by controlling for the image label Y . Here, we train a separate classifier to model $P(M|Q)$ for each of the 1000 labels in the ImageNet dataset. Each classifier is trained on the aggregate of 50 images per label along with all 15 corruptions at 5 severity levels (3751 total per label). We again use an 80/20 train/test split and perform 5-fold cross-validation. The results shown in Figure 20b are an average of the AUC over all labels and folds.

We find here that across all IQ metrics evaluated, $mAUC$ is barely above chance. For the traditional NR-IQA metrics, this supports our analysis and main experiments which show little correlation between M, Q . For the ZSCLIP-IQA metric, we refer again to the causal model (Fig. 6) and see that while the task selection variable ensures the association between M, Q , it is the conditioning on Y (and X), as done here, that blocks all paths between M, Q and once again removes the association.

H PREDICTABILITY OF DNN PERFORMANCE FOR MILDLY CORRUPTED DATASETS

To show that $D1$ is satisfied even in the case of mildly corrupted data, we plot the distributions of Q in Figure 21. Across all variants, even in cases where the likelihood is low, each IQA metric exhibits sensitivity to corruption (**D1**).

While some IQA metrics are more sensitive to the overall image corruption, this does not necessarily translate to higher predictability. In fact, ZSCLIP-IQA appears to have smaller differences in IQA distribution across variants compared to other IQA metrics, yet the highest predictability of M . Figure 22 shows the predictability of M from Q for variants of the IN-C benchmark created as described in §6.3.

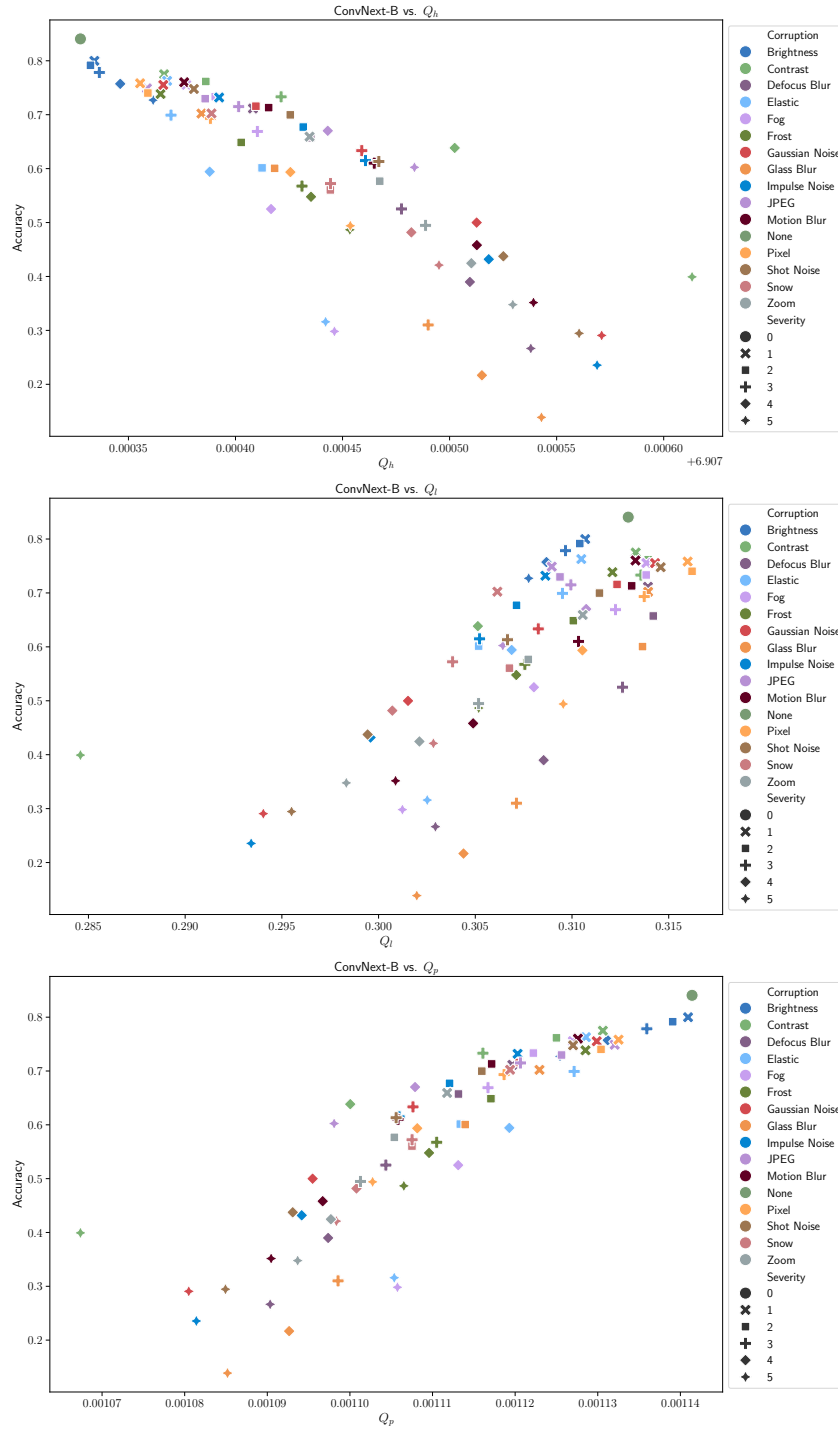


Figure 17: Comparison of ConvNext-B accuracy with (top to bottom) Q_h, Q_l, Q_p based on ZSCLIP-IQA. High correlation is observed between each ZSCLIP-IQA variant and accuracy.

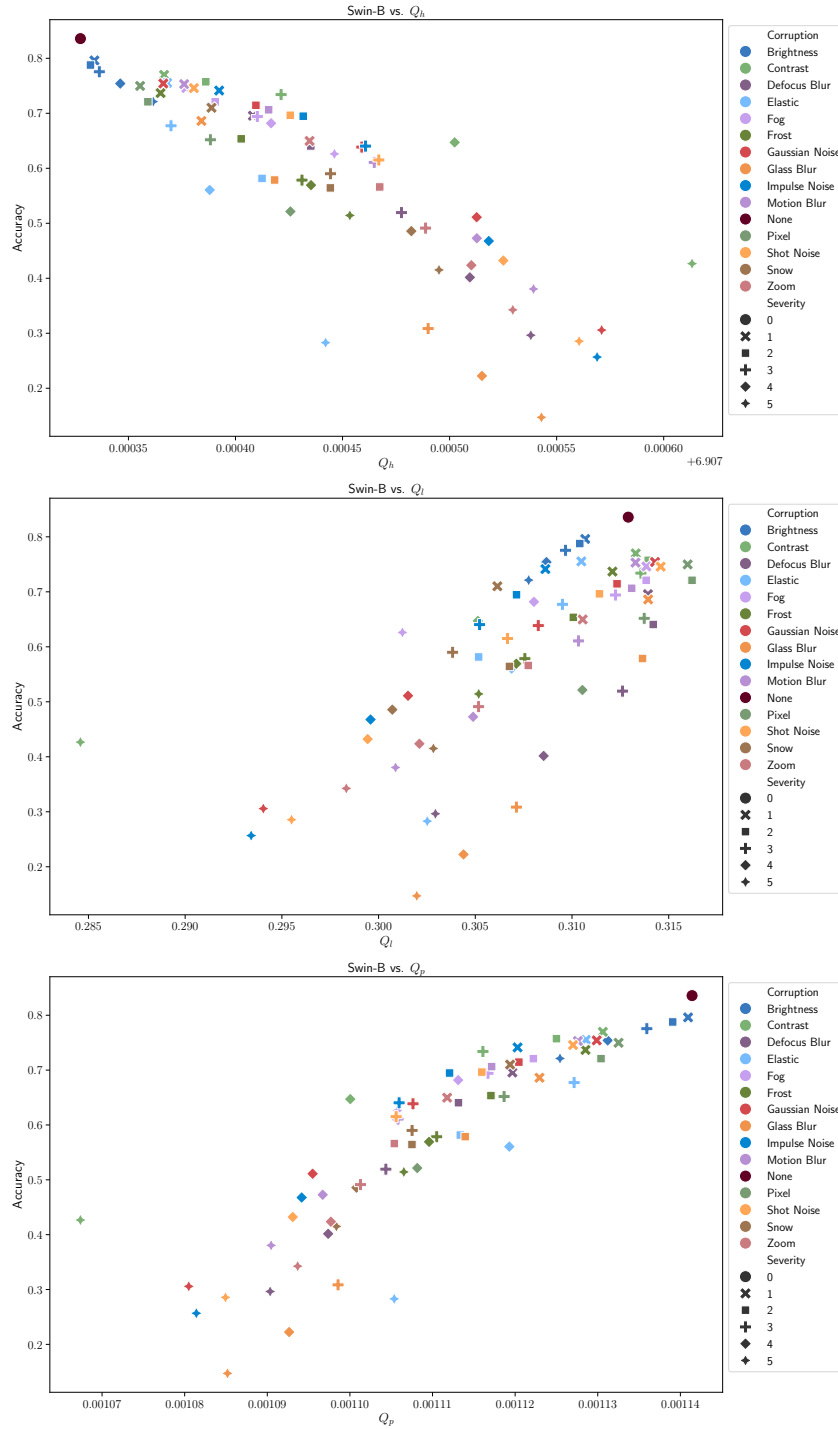


Figure 18: Comparison of Swin-B accuracy with (top to bottom) Q_h , Q_l , Q_p based on ZSCLIP-IQA. Some correlation is observed between each ZSCLIP-IQA variant and accuracy.

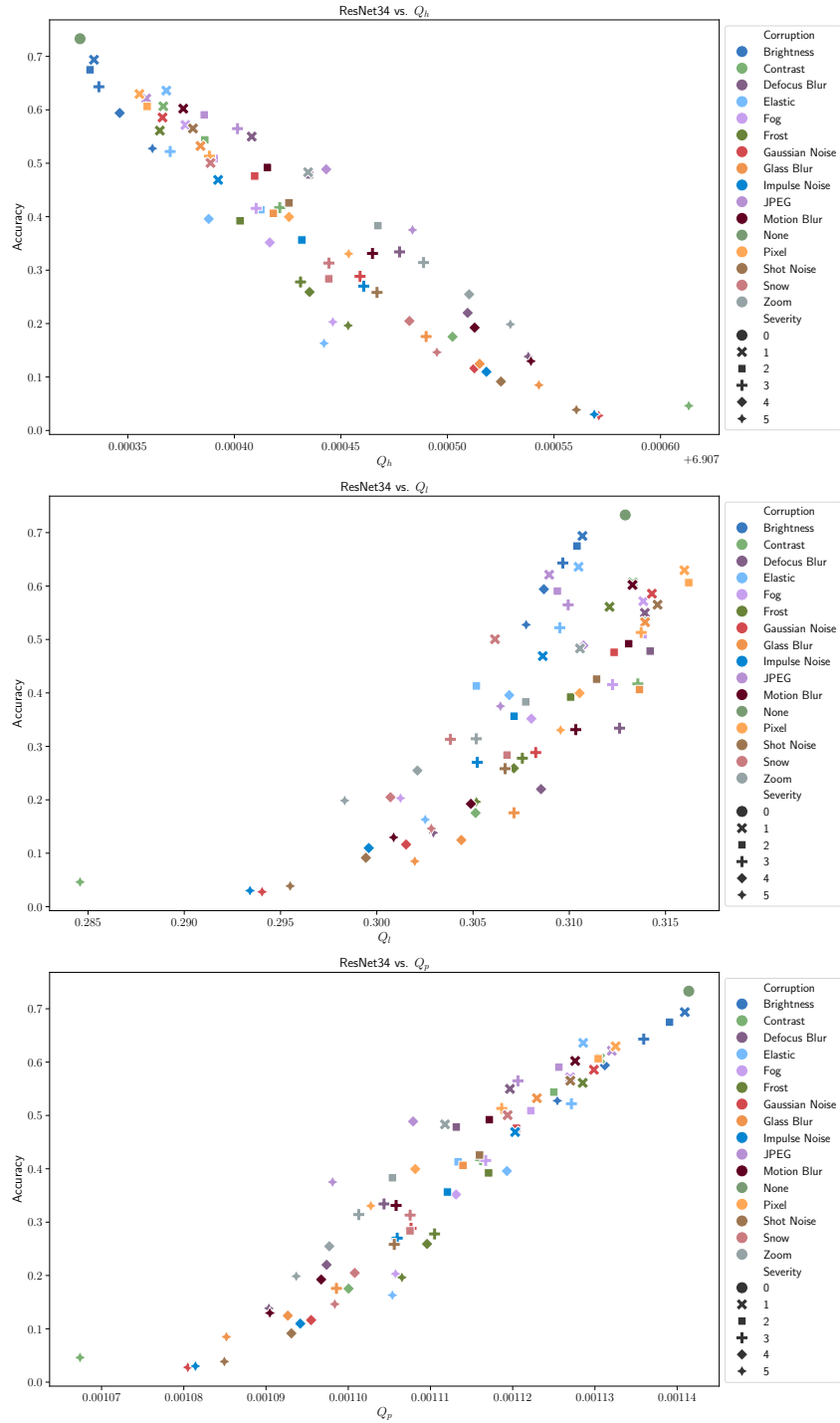


Figure 19: Comparison of ResNet34 accuracy with (top to bottom) Q_h , Q_l , Q_p based on ZSCLIP-IQA. High correlation is observed between each ZSCLIP-IQA variant and accuracy.

Table 4: Correlation between IQ and accuracy. SRCC, PLCC computed using average accuracy for each (corruption, severity). AUC and CE based on point-wise predictions (95% CI within ± 0.001). SRCC, PLCC values have $p < 0.05$.

Model	IQA Metric	AUC \uparrow	CE \downarrow		PLCC \uparrow	SRCC \uparrow
ConvNext-B	ConvNext-B Q_h	0.772	0.562		0.822 \pm 0.070	0.854 \pm 0.063
	ConvNext-B Q_l	0.778	0.555		0.826 \pm 0.067	0.854 \pm 0.063
	ConvNext-B Q_p	0.826	0.504		0.888 \pm 0.045	0.910 \pm 0.044
	ResNet34 Q_h	0.725	0.601		0.859 \pm 0.069	0.924 \pm 0.045
	ResNet34 Q_l	0.717	0.603		0.866 \pm 0.051	0.925 \pm 0.043
	ResNet34 Q_p	0.719	0.601		0.875 \pm 0.051	0.926 \pm 0.044
	Swin-B Q_h	0.760	0.579		0.624 \pm 0.165	0.724 \pm 0.170
	Swin-B Q_l	0.724	0.601		0.604 \pm 0.166	0.686 \pm 0.176
	Swin-B Q_p	0.791	0.547		0.742 \pm 0.132	0.797 \pm 0.139
ResNet34	ConvNext-B Q_h	0.767	0.557		0.858 \pm 0.060	0.889 \pm 0.055
	ConvNext-B Q_l	0.760	0.563		0.853 \pm 0.059	0.896 \pm 0.055
	ConvNext-B Q_p	0.801	0.522		0.904 \pm 0.044	0.930 \pm 0.041
	ResNet34 Q_h	0.848	0.470		0.930 \pm 0.028	0.969 \pm 0.023
	ResNet34 Q_l	0.827	0.492		0.951 \pm 0.015	0.973 \pm 0.020
	ResNet34 Q_p	0.850	0.461		0.960 \pm 0.015	0.977 \pm 0.021
	Swin-B Q_h	0.751	0.574		0.643 \pm 0.153	0.774 \pm 0.140
	Swin-B Q_l	0.709	0.600		0.628 \pm 0.146	0.754 \pm 0.145
	Swin-B Q_p	0.774	0.551		0.747 \pm 0.129	0.825 \pm 0.112
Swin-B	ConvNext-B Q_h	0.744	0.586		0.706 \pm 0.129	0.768 \pm 0.098
	ConvNext-B Q_l	0.746	0.586		0.709 \pm 0.127	0.768 \pm 0.099
	ConvNext-B Q_p	0.791	0.542		0.788 \pm 0.102	0.834 \pm 0.079
	ResNet34 Q_h	0.722	0.603		0.828 \pm 0.078	0.896 \pm 0.053
	ResNet34 Q_l	0.713	0.604		0.831 \pm 0.061	0.892 \pm 0.053
	ResNet34 Q_p	0.716	0.602		0.845 \pm 0.062	0.897 \pm 0.052
	Swin-B Q_h	0.766	0.578		0.483 \pm 0.207	0.654 \pm 0.174
	Swin-B Q_l	0.732	0.597		0.458 \pm 0.203	0.611 \pm 0.181
	Swin-B Q_p	0.807	0.529		0.620 \pm 0.184	0.732 \pm 0.142

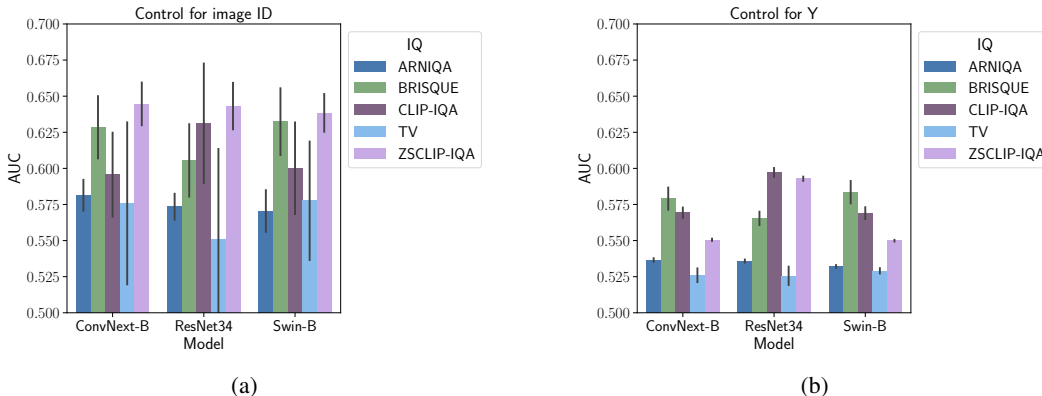


Figure 20: Mean AUC (mAUC) for classifiers trained (a) per image ID (X_i) to model $P(M|Q, X_i)$ and (b) per label Y to model $P(M|Q, Y)$. Averages are taken over all images/labels respectively and cross-validation folds with error bars indicating one standard deviation. Higher variance in (a) is attributed to lower sample sizes for training the logistic regression classifier.

Results show that weak task-guided IQA metrics are able to achieve higher AUC even when the number of corrupted images in the dataset is low. In comparison, conventional NR-IQA metrics achieve lower AUC and are more sensitive to the total level of corruption.

I COMPUTE RESOURCES

All experiments were run using a single NVIDIA A40 GPU with 48GB of memory. Predictability analysis can be conducted on CPU-only machine with at least 8 cores.

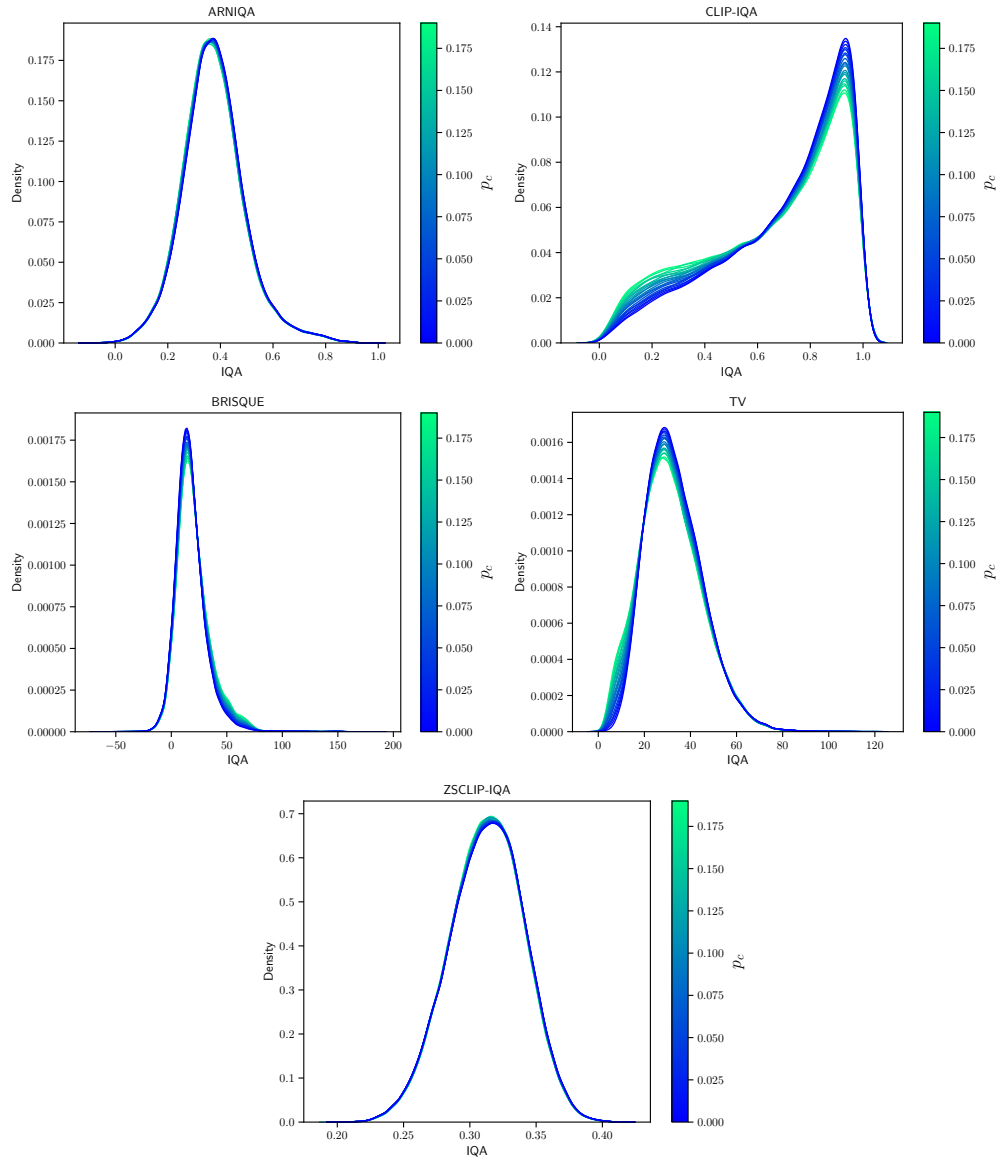


Figure 21: Distribution of IQA for each mildly corrupted variant of IN-val. Line color indicates the likelihood of image corruption p_c for each variant. Note that the amount of similarity/difference in the IQA distribution across variants does not explain the predictability which is determined by the causal DAG such as in §3, §5, and §6. See Figure 22 for predictability results.

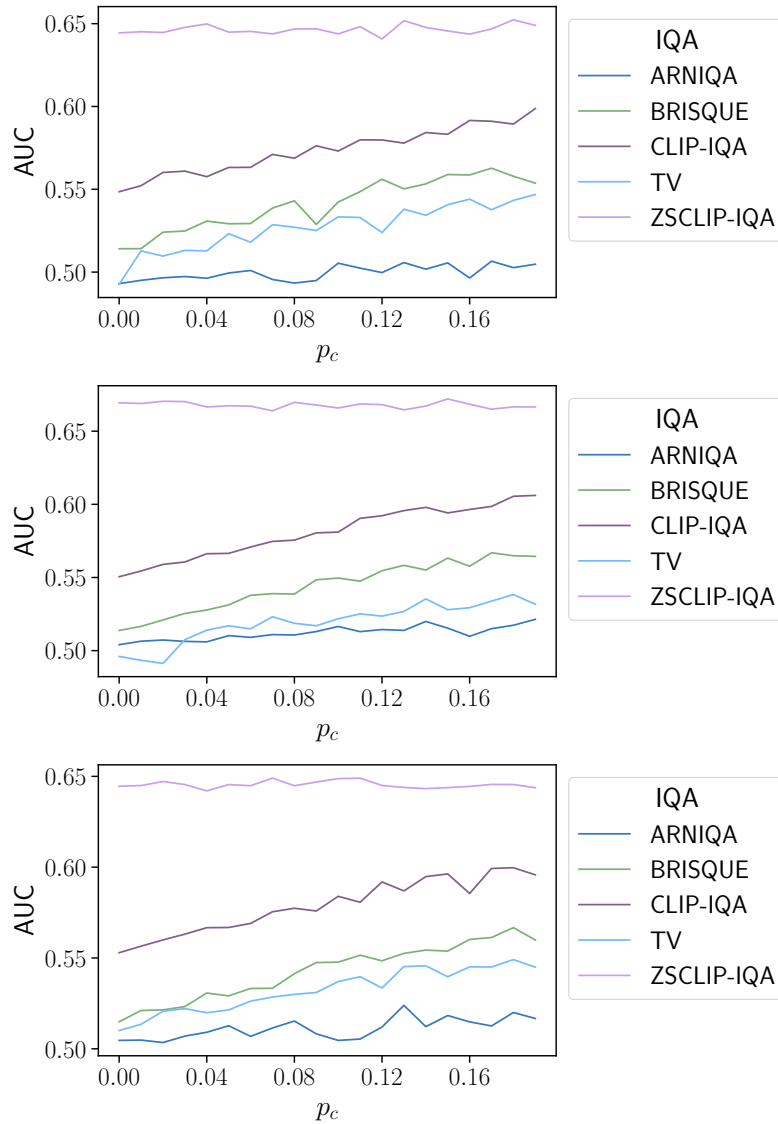


Figure 22: AUC vs. p_c where p_c represents the fraction of images in the test set that are mildly corrupted. Results are listed top to bottom: ConvNet-B, ResNet34, Swin-B. Predictability for ZSCLIP-IQA is relatively insensitive to the proportion of corrupted images whereas other metrics only improve as the proportion and diversity of corruptions increases.